Scaling Behavior of Convective Mixing, with Application to Geological Storage of CO_2

Hassan Hassanzadeh, Mehran Pooladi-Darvish, and David W. Keith
Dept. of Chemical and Petroleum Engineering, University of Calgary, Calgary, AB, Canada T2N 1N4

DOI 10.1002/aic.11157
Published online March 21, 2007 in Wiley InterScience (www.interscience.wiley.com).

CO_2 storage in deep saline aquifers is considered a possible option for mitigation of greenhouse gas emissions from anthropogenic sources. Understanding of the underlying mechanisms, such as convective mixing, that affect the long-term fate of the injected CO_2 in deep saline aquifers, is of prime importance. We present scaling analysis of the convective mixing of CO_2 in saline aquifers based on direct numerical simulations. The convective mixing of CO_2 in aquifers is studied, and three mixing periods are identified. It is found that, for Rayleigh numbers less than 600, mixing can be approximated by a scaling relationship for the Sherwood number, which is proportional to $Ra^{1/2}$. Furthermore, it is shown that the onset of natural convection follows $t_{Dc} \sim Ra^{-2}$ and the wavelengths of the initial convective instabilities are proportional to Ra. Such findings give insight into understanding the mixing mechanisms and long term fate of the injected CO_2 for large scale geological sequestration in deep saline aquifers. In addition, a criterion is developed that provides the appropriate numerical mesh resolution required for accurate modeling of convective mixing of CO_2 in deep saline aquifers. *AIChE J,* 53: 1121–1131, 2007
Keywords: scaling, convective mixing, CO_2 storage or sequestration, deep saline aquifers, numerical simulation

Introduction

In CO_2 geological storage, CO_2 is injected into a deep saline aquifer that has a cap rock. The injected CO_2 is typically less dense than the resident brines. Driven by buoyancy, CO_2 will flow laterally and upward, spreading under the cap rock. During CO_2 migration, a portion of the CO_2 is trapped as a residual saturation. The free phase CO_2 (usually a supercritical fluid) may flow upwards, potentially leaking through any high permeability zones or artificial penetrations, such as abandoned wells. The free-phase CO_2 slowly dissolves in formation water. The resulting CO_2-rich brine is slightly denser than the undersaturated brine, potentially leading to natural convection.[1] The convective mixing improves CO_2 dissolution by continuously removing CO_2-saturated water from the region adjacent to the CO_2 on top and bringing undersaturated water into contact with the CO_2 plume. Correct estimation of the rate of dissolution is important because the timescale for dissolution corresponds to the timescale over which free phase CO_2 has a chance to leak out.

Natural convection in porous media has been studied rather extensively.[2] However, in the framework of CO_2 storage, stability analysis of a gravitationally unstable, CO_2-rich brine diffusive boundary layer has been investigated only more recently.[3–7] Ennis-King et al. (2005) and Ennis-King and Paterson (2005) performed a linear stability analysis to investigate the role of anisotropy with respect to the onset of convection.[3,4] Riaz et al. (2006) used linear stability analysis based on the dominant mode of the self-similar diffusion operator to find a scaling relationship for the onset of natural convection.[5] Xu et al. (2006) also used linear stability analysis and developed a scaling relationship for the onset of convection.[6] Hassanzadeh et al. (2006) studied the effect of various boundary and initial conditions on the onset of

Correspondence concerning this article should be addressed to M. P. Darvish at pooladi@ucalgary.ca.

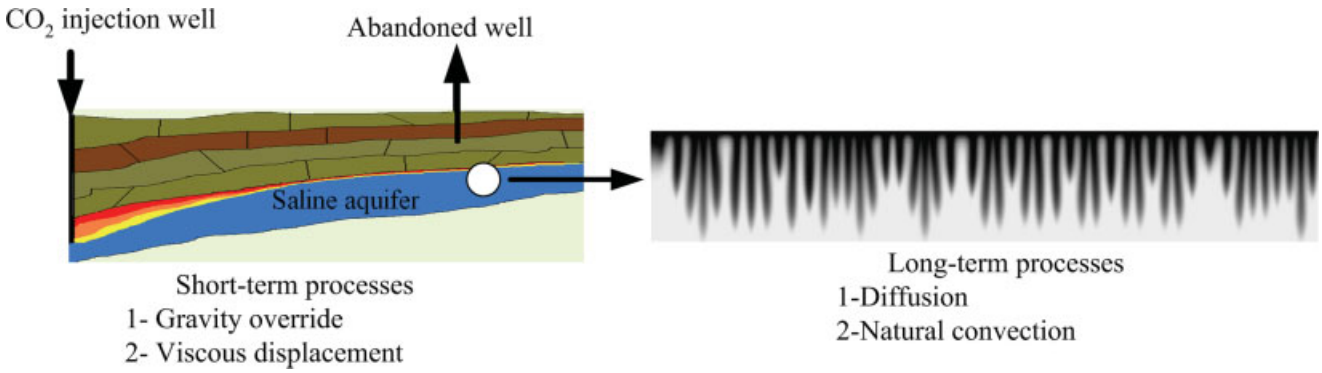

Figure 1. A schematic of CO_2 injection into a deep saline aquifer describing some of the short-term and long-term processes involved in geological storage of CO_2.

[Color figure can be viewed in the online issue, which is available at www.interscience.wiley.com.]

convection in a homogenous and isotropic porous medium using linear stability analysis.[7] However, the stability analysis used in previous works only determines the onset of marginal instability and *cannot* be used to evaluate the mixing behavior *after* the onset of convection. Such results can be found directly only by using numerical simulations. In this paper, we indeed use a numerical model to extend our previous theoretical analysis to characterize the mixing mechanism after the onset of convection.[7,8] In the study, we perform numerical simulations to obtain scaling relationships for the onset of convection, mixing periods, and also maximum Sherwood number for predicting the rate of dissolution. Such scaling gives insight into screening and selection of suitable candidates for storage sites that assist in the characterization and implementation of large scale CO_2 storage in deep saline aquifers.

This article is structured as follows. First, the numerical simulation of the mixing mechanism is presented and described. Next, scaling relationships for the onset of convection, initial wavelength of the convective instabilities, mixing periods, and the Sherwood number are presented. Then, application of the developed scaling methodology to some of the Alberta basin aquifers is presented, followed by discussion and conclusions.

Description of the Problem

Figure 1 illustrates some of the short- and long-term processes involved in CO_2 storage in deep saline aquifers. Short-term processes include gravity override of CO_2 and viscous immiscible displacement, and generally have timescales of years to decades. On the other hand, long-term processes such as diffusion and convection have century-long timescales. Diffusion of CO_2 into the underlying formation brines might cause convection. Correct estimation of the rate of dissolution of CO_2 into formation brines is important because the timescale for that dissolution is the timescale over which CO_2 has a chance to leak through pathways such as fractures, faults, and abandoned wells. In the following, we present numerical simulations of convective mixing.

The physical model, coordinate system, and boundary conditions used in numerical simulations are shown in Figure 2. The model is an isotropic and horizontal porous layer of thickness H, saturated with formation water. Boundary conditions are no fluid flow across all boundaries at all times, no mass fluxes across lateral and bottom boundaries at all times, and constant concentration at the top boundary for time greater than zero. The fluid is initially quiescent and the porous medium is homogenous in terms of porosity and permeability. The domain is exposed to a rapid change in CO_2 aqueous concentration at the top at time zero. Because of diffusion of CO_2 into the brine, the brine becomes saturated with CO_2 and gains a density higher than fresh water. It is well known that a top heavy arrangement is unstable to certain perturbations when the Rayleigh number exceeds a critical value. The Boussinesq approximation and Darcy flow model are assumed valid. Furthermore, we assume that velocity-based dispersion and capillary effects are negligible and that geochemi-

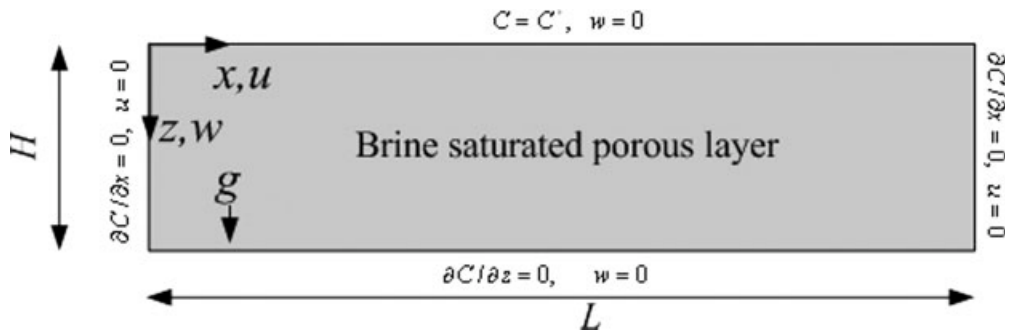

Figure 2. Geometry and boundary conditions used in the numerical simulations.

cal reactions are not present. For such a system, the governing equations of flow and concentration fields expressed by employing the Darcy model for velocity are given by[9]:

$$\nabla \cdot \mathbf{v} = 0, \tag{1}$$

$$\mathbf{v} = -\frac{k}{\mu}(\nabla p - \rho g \nabla z), \tag{2}$$

$$D\phi\nabla^2 C - \mathbf{v} \cdot \nabla C = \phi \frac{\partial C}{\partial t}, \tag{3}$$

where $\rho = \rho_0 (1 + \beta C)$, $\mathbf{v}$ is the vector of Darcy velocity, t is time, k is permeability, ϕ is porosity, p is pressure, C is concentration, ρ_0 is pure water density, μ is viscosity, β is the coefficient of density increase with concentration, and D is the molecular diffusion coefficient. Using linear stability analysis, one can estimate the onset of convection and the initial wavelength of the convective instabilities. However, as noted earlier, estimation of the mixing behavior after the onset of convection is not possible by linear stability analysis. Here, we use a numerical simulation of the convective mixing using the formulation given by Eqs. 1–3.

The important parameter to describe the stability of such a system is the porous medium Rayleigh number, defined by[10,11]:

$$\mathrm{Ra} = \frac{kg\Delta\rho H}{\mu\phi D}, \tag{4}$$

where $\Delta\rho = \beta\rho_0 C^*$ is the density difference and C^* is the CO_2 equilibrium concentration at initial pressure. The total amount of CO_2 that can be dissolved to saturation in the formation brine is given as $c = V_p C^*$, where V_p is the aquifer pore volume. In the following sections, high resolution numerical simulations are presented. In all simulations, the fluid and porous medium are assumed to be incompressible and the initial CO_2 concentration within the model was set to zero.

Numerical Analysis of the Problem

Numerical simulations of density-driven flow are highly prone to discretization error. Therefore, care should be taken to obtain accurate solutions. Numerical solutions are typically oscillation free and the numerical error is small for $P_E \leq 2$ and $C_R \leq 1$, where C_R and P_E are grid Courant and Peclet numbers, respectively. Therefore, the main criteria for the stability and accuracy of the finite difference method applied to transport equation are given by[12,13]:

$$C_R = v_l \frac{\Delta t}{\phi \Delta l} \leq 1, \quad P_E = v_l \frac{\Delta l}{D\phi} \leq 2, \tag{5}$$

where v is the Darcy velocity, Δl ($l = x, z$) is the grid block size, and Δt is the simulation time step. In addition to these constraints, it has been suggested that, for a multidimensional problem, the following condition should also be satisfied[12,13]:

$$C_R = \frac{v_l \Delta t}{\phi \Delta l} \leq \frac{P_E}{2}. \tag{6}$$

In the numerical simulations presented, the maximum time step is calculated based on the Courant number criterion given by Eq. 5 and the above criteria are honored in all simulations. In all cases, the grid block sizes are chosen such that they are at least 20 times smaller than the initial wavelength of the convective instabilities obtained by linear stability analysis.[7]

One can also define the maximum velocity in the vertical direction, based on the maximum density difference, as given by[14,15]:

$$v_{\max} = \frac{k}{\mu}\Delta\rho g. \tag{7}$$

Substituting for a maximum velocity in the Peclet number definition, and knowing that $H = n_z \Delta z$, results in $P_{E\max} = \mathrm{Ra}/n_z$, where n_z and Δz are the number and size of the grid blocks in vertical direction, respectively. From numerical solutions, we found that, for the problem under consideration, the ratio of maximum grid Peclet number and the actual grid Peclet number that gives an accurate solution is $\leq$3.5. Substituting for the grid Peclet number criterion gives $\mathrm{Ra}_G \leq 7$, where Ra_G (the grid block Rayleigh number) is given by $\mathrm{Ra}_G = k\Delta\rho g \Delta z/\phi\mu D$. The criterion of $\mathrm{Ra}_G \leq 7$ gives the minimum number of grid blocks necessary for accurate modeling of the convective mixing process in geological storage of CO_2.

In the following section, mixing mechanisms and mixing regimes are described.

Mixing Mechanisms and Mixing Regimes

Convective mixing has been identified as a CO_2 dissolution mechanism in geological storage of CO_2 for more than a decade,[1] but the associated mass transfer mechanism has not been characterized. In this section, we describe and characterize the mixing process for the first time based on our numerical simulation results. The general behavior of the mixing process is described first. For a closed aquifer, the total amount of CO_2 dissolved at any time, divided by the ultimate amount of CO_2 dissolution, is defined as the fraction of ultimate dissolution.[16] Figure 3a shows a typical mixing curve that includes diffusion and convection curves. The convective mixing curve can be divided into three periods including: (A) *diffusive mixing*, (B) *early convective mixing*, and (C) *late convective mixing*. In order to characterize the different periods of mixing, we use the Sherwood number (Sh), which is defined as the ratio of total mixing to mixing achieved by pure diffusion.[17] Figure 3b shows a typical variation of the Sherwood number versus time for the problem under consideration. Part "A" is a period where the dominant process is diffusion, and the rate of dissolution is slow and depends on the molecular diffusion coefficient. The distance traveled by a diffusion front is called "penetration depth." The diffusion penetration depth follows the Einstein-type relation given by $\delta_D \propto \sqrt{t_D}$,[17–19] where the dimensionless time is defined as $t_D = Dt/H^2$. Since during early times, the dominant mechanism is molecular diffusion, and the penetration depth is small, the total mass transfer is proportional to $t_D^{1/2}$. The fraction of ultimate dissolution (mixing) during this period for the problem illustrated in Figure 2 can be obtained using the following equation[20]:

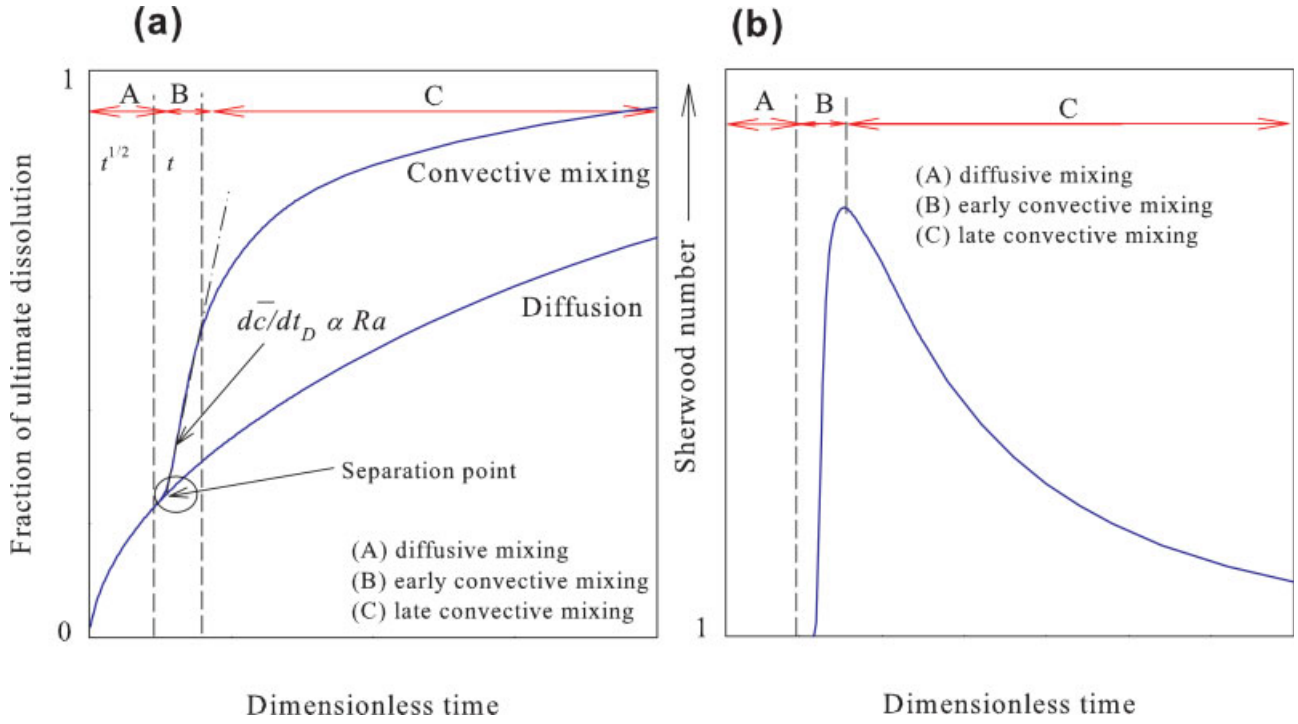

Figure 3. Typical dissolution (a) and Sherwood number (b) curves for convective mixing.

[Color figure can be viewed in the online issue, which is available at www.interscience.wiley.com.]

$$\bar{c} = 1 - \frac{8}{\pi^2}\sum_{n=0}^{\infty}\left(\frac{1}{2n+1}\right)^2 \exp\left[-\left(\frac{2n+1}{2}\pi\right)^2 t_D\right]. \quad (8)$$

The duration of this period depends on the aquifer Rayleigh number and is limited by the onset of convection. For some aquifers, the mass transfer mechanism remains diffusive, until the diffusive front reaches the bottom boundary. Beyond this time, total mixing is no longer proportional to $t_D^{1/2}$. For a system where convective instability does not develop, the Sherwood number is unity and the only acting mechanism is pure diffusion, as shown in Figure 3b. After an initial diffusive period, where the penetration depth grows with $t_D^{1/2}$, the diffusive boundary layer might become unstable, being approximately coincident with the time of the onset of convection. Numerical simulations have confirmed that the onset of convection occurs shortly before the departure of the convective mixing curve from the pure diffusion curve as shown in Figure 3a.

In part "B," the concentration boundary layer becomes unstable and leads to the generation of growing instabilities at the interface, which are related to the physical properties of the fluid and porous medium. Mixing during this period is dominated by the convective growth of the instabilities. It is therefore expected that, during this period, mixing is directly proportional to time as shown in Figure 3a. To examine the hypothesis and to determine the proportionality constant, the calculated dimensionless rate of mixing of CO_2 in brine ($d\bar{c}/dt_D$) after the separation point of convective mixing and diffusive mixing curves is shown in Figure 4 as a function of Rayleigh number. Results reveal that the dimensionless rate of mixing is independent of time, implying that mixing is proportional to time. Furthermore, the results shown in Figure 4 indicate that the dimensionless rate of mixing after

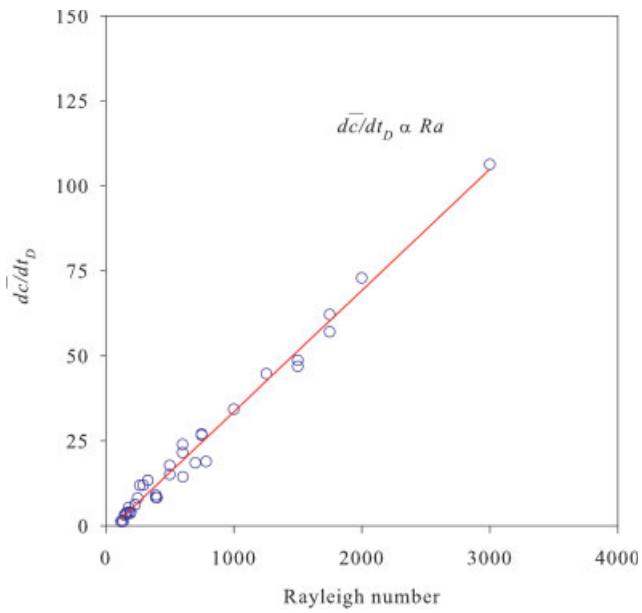

Figure 4. Dimensionless rate of mixing of CO_2 as a function of Rayleigh number during early stage of the second period of mixing (period B).

[Color figure can be viewed in the online issue, which is available at www.interscience.wiley.com.]

Table 1. Parameters Used for Simulation of Convective Mixing

Case	H (m)	L (m)	D (m^2/s)	$\Delta\rho$* (kg/m^3)	ϕ	μ (cp)	K (mD)	Ra
1	0.125	1.25	2×10^{-9}	20	0.1	0.5	800	196
2	0.04	0.2	2×10^{-10}	20	0.1	0.5	1000	392
3	6	15	2×10^{-9}	20	0.1	0.5	80	943

*Density difference between CO_2 saturated brine and fresh brine.

separation of convective and diffusive curves is directly proportional to the system Rayleigh number. However, throughout this period and in particular for large Rayleigh numbers, interaction of the growing convective fingers could take place, which might change the rate of mixing. For smaller Rayleigh numbers, the diffusive penetration depth ahead of the instability fingers reaches the bottom boundary, such that the effect of the finger interaction does not affect the mixing and the system is bottom-boundary dominated. However, for large Rayleigh numbers, interaction between fingers might have a strong effect on the mixing process. Depending on the system Rayleigh number, the rate of dissolution in this period is higher than the pure diffusion process, and the fraction of ultimate dissolution could reach >50% by the end of the period.

Once the effect of the bottom boundary becomes important, the dissolution curve deviates from direct proportionality to time and the rate of mixing begins to decrease with time. This is the beginning of period "C" and is characterized by the maximum Sherwood number as presented in Figure 3. Convective mixing distributes the dissolved CO_2 into the aquifer and stratifies the density gradients. Stratification of the density gradients diminishes the convection velocity and leads to a lower rate of dissolution in period "C." During this period, density gradients diminish and the convection cells gradually die down. The time periods of mixing and the maximum Sherwood number described above are helpful for screening storage sites for large scale implementation of geological CO_2 storage. As mentioned, for a diffusion-dominated system, the governing equations are linear and can be solved analytically. However, for systems dominated by convection, the differential equations are nonlinear and do not allow analytical solutions. Highly refined numerical solutions have been used to simulate such non-linear equations. In the next section, we show that scaling relationships can be obtained from direct numerical simulations, which would allow determination of the rate of mixing. In the future, such simple scaling relationships can then be used to estimate the mixing without the need for additional, highly computationally expensive numerical simulations. The detailed equations for determining the mixing periods are presented subsequent to the study of finger growth in the following section.

The problem geometry and data used in numerical simulations are given in Figure 2 and Table 1, respectively. Figure 5 shows the calculated concentration maps for the three resulting Rayleigh numbers at different stages of mixing. At low Ra, high-concentration fingers move downward freely with almost no interaction with neighboring fingers, while at higher Rayleigh numbers, finger interactions retard their downward movement. Finger interactions occur both at low and high Rayleigh numbers. At low Rayleigh numbers, interaction is limited only to cross diffusion between fingers, while at high Rayleigh numbers, both cross diffusion and more complex finger interaction contribute to the mixing mechanisms. The initial wavelengths (λ) of the convective instabilities obtained from numerical solutions are compared with those from the linear stability analysis. For Ra = 196, the linear stability analysis predicts 15.61 fingers compared to a numerical value of 16.5, as shown in Figure 5a for a dimensionless time of 0.0646. Similarly, for Ra = 392, the linear stability analysis predicts 15.6 fingers compared to a numerical value of 15.5, as depicted in Figure 5b for a dimensionless time of t_D =0.0202. At Ra = 943, numerical simulation predicts 16 fingers compared to 18 fingers from the linear stability analysis at a dimensionless time of 0.0035.

In the following, a measure of the effectiveness of the mixing process is presented in terms of the fraction of ultimate dissolution and maximum Sherwood number as a function of time. Figures 6a, b demonstrate the fraction of ultimate dissolution as compared with pure diffusion and Sherwood number versus dimensionless time of mixing for Rayleigh numbers of 196 and 392. Results demonstrate that, in both cases at the time of maximum Sherwood number, >50% of the ultimate dissolution is achieved, where the dissolution achieved by pure diffusion is less than 30%. The ratio of diffusion time to convective mixing time as a function of dissolution for the two Rayleigh numbers is shown in Figures 6c, d. Results show that convective mixing dissolves large amounts of CO_2 in formation brine in a shorter period of time than what would be achieved with the pure diffusion mechanism, which is an expected result.

Scaling Analysis of Convective Mixing

Onset of natural convection

In this section, numerical simulations are presented to find the onset of convection in an isotropic and homogenous, saturated porous layer, which is closed all around and exposed to constant concentration from the top. The CO_2-brine interface is considered as a boundary condition to avoid two-phase flow complications. Numerical simulations (30 cases) were performed by varying the molecular diffusivity, model thickness, and porous medium permeability by three orders of magnitude, resulting in a wide range of Rayleigh numbers. The numerical solutions were obtained without imposing physical perturbations. Numerical artifacts such as truncation errors trigger instabilities. In all cases, the grid Peclet and Courant number criteria were honored and the grid block sizes were chosen such that they were at least 20 times smaller than the wavelength of the convective instabilities obtained from the linear stability analysis method.

The dimensionless group used in the scaling is the Rayleigh number. Linear stability analysis suggests that Ra should be larger than certain critical values for convection to initiate.[10,11] In addition, using stability analysis, it has been found[3–7] that the time to onset of convection can be represented by $t_{Dc} = c_1 Ra^{c_2}$, where c_1 and c_2 are constants and t_{Dc} is the dimensionless critical time scaled by the diffusion time-scale, H^2/D. The dimensionless time t_{Dc} represents the end of the diffusion dominated period "A" and the start of period "B" as described by Figure 3.

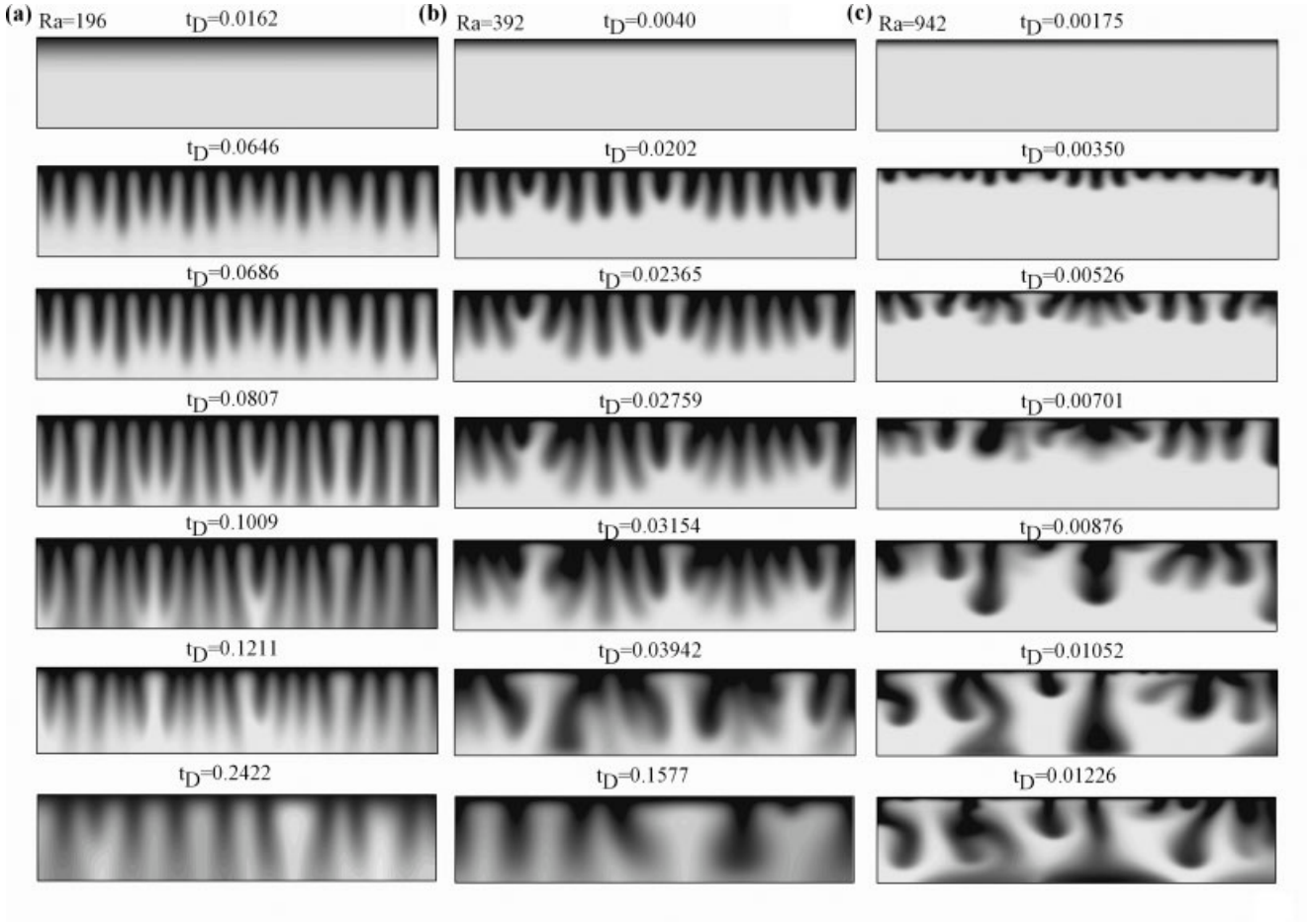

Figure 5. Evolution of convective mixing fingers for three cases with (a) Ra = 196, (b) Ra = 392, and (c) Ra = 942 at different periods of mixing, where darker color means higher concentration.

The time at which the diffusive boundary layer becomes unstable is marked as the onset of convection. Figure 7 shows the onset of convection (i.e. the dimensionless critical time) as a function of the Rayleigh number obtained from numerical simulations. Results presented in Figure 7 show that, at large Rayleigh numbers, the dimensionless time to onset of convection is inversely proportional to the square of the Rayleigh number. Since the dimensionless time is inversely proportional to the porous layer thickness to the power of two and the Rayleigh number is proportional to the layer thickness, the dimensional time to the onset of convection is therefore independent of the porous layer thickness. As shown in Figure 7, similar scaling behavior has been reported by previous studies using linear stability analysis methods.[3–7] In Figure 7, the numerical dimensionless time for the onset of instability can be written as $t_{Dc} = 500/Ra^2$ ($c_1 = 500$, $c_2 = -2$), which can be expressed in terms of physical parameters by:

$$t_c = 500\left(\frac{\phi\mu\sqrt{D}}{k\Delta\rho g}\right)^2, \tag{9}$$

where t_c is critical time in seconds.

Depending on the choice of analytical approach, initial conditions, and stability criterion used, different c_1 values have been reported in the literature.[3–7] In order to avoid using the assumptions that have been made in these analytical treatments, we used direct numerical simulations to find the time to onset of convection. Results reveal that the time for onset of convection obtained based on direct numerical simulations obey similar scaling behavior when compared with that from linear stability analysis approach with a c_1 value that is larger than those obtained from linear stability analysis. From a practical standpoint, onset of instability signals beginning of increased dissolution through convective mixing (increased Sherwood number). However, our numerical results show that the Sherwood number remain almost constant for some time after the time to onset of convection. Therefore, and for practical applications when this improved mixing (i.e. increase in the Sherwood number) is of importance, we suggest using larger values of c_1 obtained through numerical computations reported here.

Initial wavelength of the convective instabilities

The wave numbers of the initial convective instabilities as a function of Rayleigh number are compared with those obtained from linear stability analysis,[7] as shown in Figure 8. The scaling relationship obtained from numerical simulation

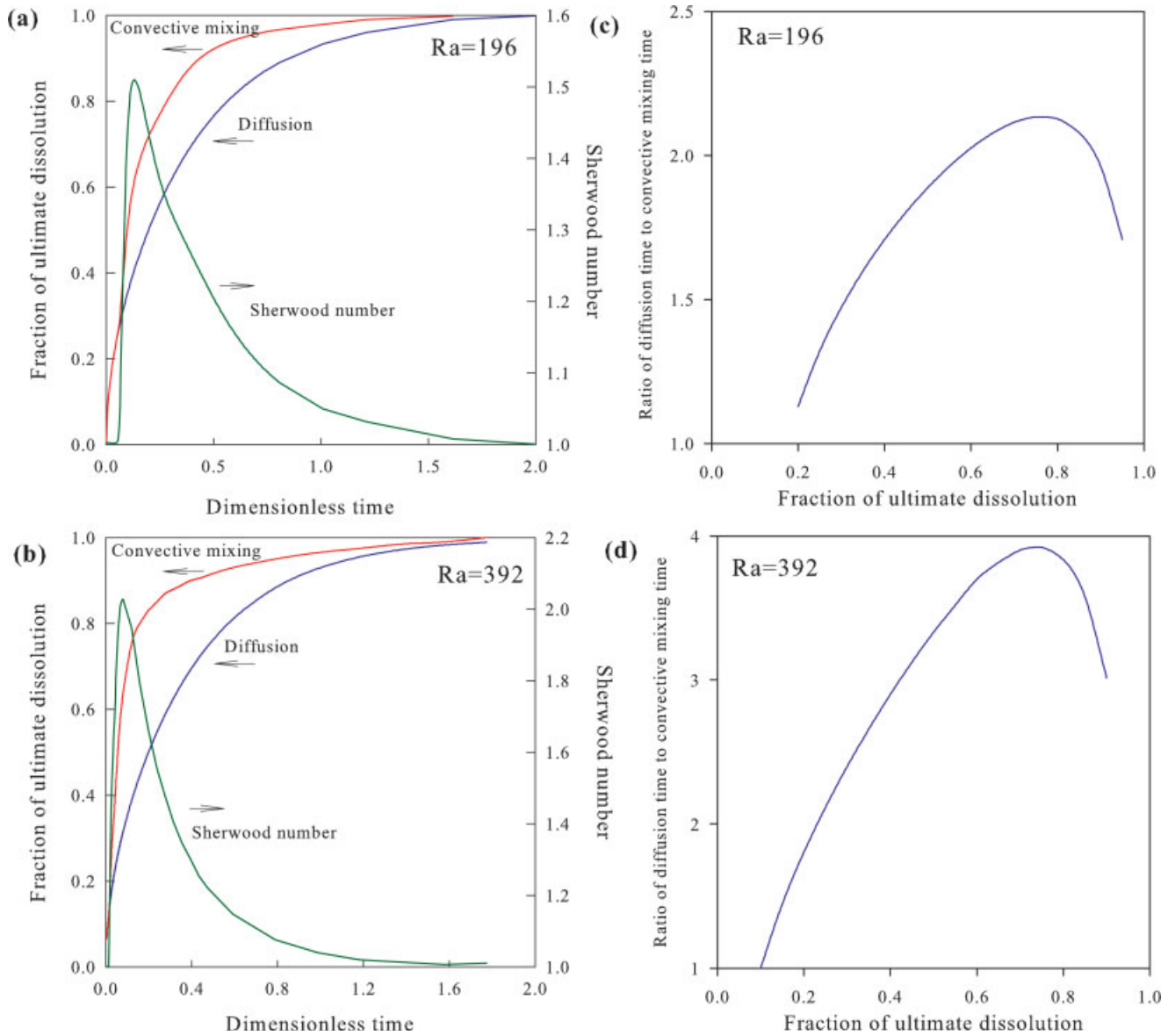

Figure 6. Dissolution and Sherwood number curves for two cases with (a) Ra = 196 and (b) Ra = 392 as a function of dimensionless time; the ratio of diffusion time to convective mixing time as a function of dissolution for the two Rayleigh numbers is shown on the right (c,d).

[Color figure can be viewed in the online issue, which is available at www.interscience.wiley.com.]

is in good agreement with the linear stability analysis. Results demonstrate that, at high Rayleigh numbers, the wave numbers are proportional to the Rayleigh number, implying that the wavelength of the initial instabilities is independent of the aquifer thickness. The scaling relationship can be expressed as $a = 0.05$ Ra, where $a = 2\pi H/\lambda$ is the dimensionless wavenumber. The wavelength of the initial convection instabilities is therefore given by:

$$\lambda = 40\pi \frac{\phi \mu D}{k \Delta \rho g}, \tag{10}$$

where λ is in meters.

Mixing periods and total mixing

The onset of convection corresponds to the end of the diffusive mixing period "A" as described by Eq. 9. The second period of mixing is the early convective mixing period "B." The time at the end of the early convective mixing period is determined by the maximum Sherwood number. Figure 9 shows the variation of Sherwood number versus time for different Rayleigh numbers. The plot of the loci of maximum Sherwood numbers versus time, and their corresponding time, characterizes the end of early convective mixing period "B." Figure 10 shows the time at the end of early convective mixing period "B" versus Rayleigh number which can be expressed by:

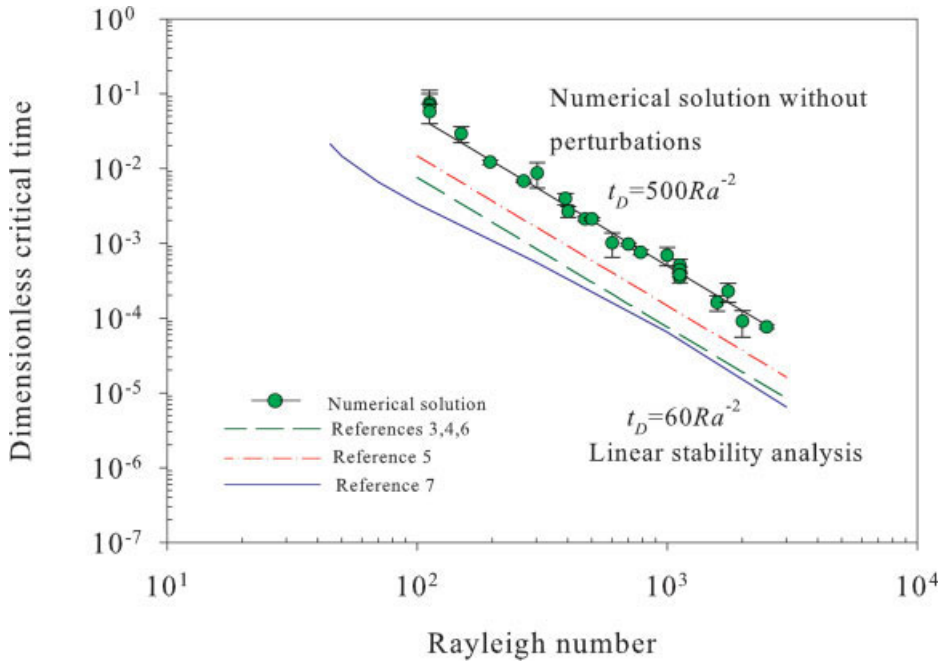

Figure 7. Onset of convection as a function of Rayleigh number obtained from numerical simulations as compared with linear stability analysis.[3–7]

[Color figure can be viewed in the online issue, which is available at www.interscience.wiley.com.]

$$t_{D\,Sh_{max}} = \frac{100}{Ra^{6/5}}. \tag{11}$$

Results presented in Figure 11 show that the maximum Sherwood number as a measure of mixing versus Rayleigh number can be expressed by the following scaling relationship for Rayleigh number less than 600:

$$Sh_{max} = 0.105Ra^{1/2}. \tag{12}$$

Results in Figure 11 also show that, at high Rayleigh numbers, the Sherwood number deviates from the scaling presented, suggesting that the scaling is not applicable for Ra > 600. This is because, at high Rayleigh numbers, the nonlinear finger interactions become more important than the effect of

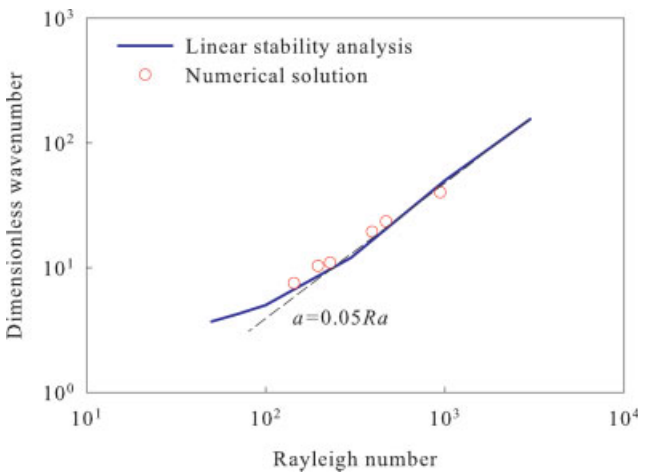

Figure 8. Dimensionless wavenumber of initial convective instabilities from numerical simulation as compared with those obtained by linear stability analysis.

[Color figure can be viewed in the online issue, which is available at www.interscience.wiley.com.]

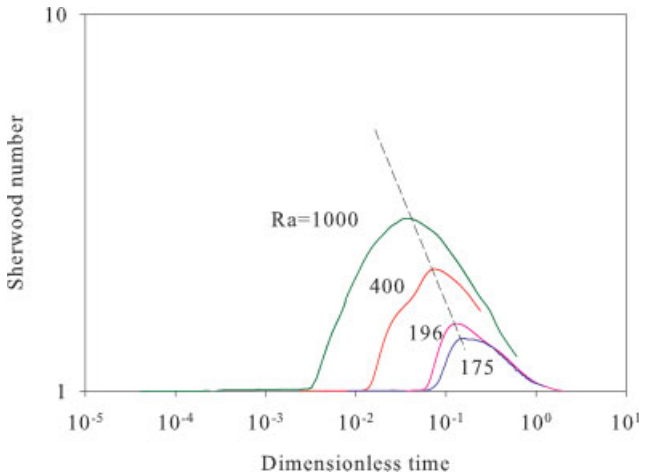

Figure 9. Sherwood number for different cases studied as a function of dimensionless time; the dashed line shows the loci of the maximum Sherwood numbers obtained from numerical solution.

[Color figure can be viewed in the online issue, which is available at www.interscience.wiley.com.]

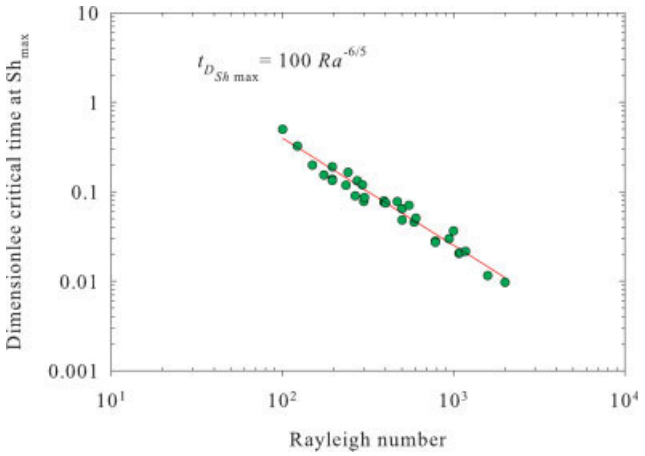

Figure 10. Dimensionless time to end of intermediate mixing period for different cases studied as a function of Rayleigh number.

[Color figure can be viewed in the online issue, which is available at www.interscience.wiley.com.]

the bottom boundary, causing the Sherwood number to deviate from the straight line in Figure 11. It was observed (Figure 5) that, at low Rayleigh numbers, fingers travel toward the bottom boundary more easily than at high Rayleigh numbers, where the complex finger interactions retard the downward movement of the fingers. Retardation of the downward movement of fingers at high Rayleigh numbers affects the mixing process and, as noted, causes deviation from the straight line of the relationship between the maximum Sherwood number and the Rayleigh number as expressed by Eq. 12.

Once the fingers touch the bottom boundary, the aquifer becomes finite with respect to the mixing process and the finger interactions become less important than the bottom boundary effect. The time at maximum Sherwood number given in Figure 10 corresponds to the start of boundary-dominated flow. Therefore, it is useful to find the penetration depth of the diffusive boundary layer at this time. The dimensionless diffusion penetration depth,[17,19] $\delta_D \approx 4\sqrt{t_D}$, is calculated at the time when the Sherwood number is at its maximum for all cases. Results reveal that, for all cases that follow the scaling, the diffusion penetration depth is larger than 0.07. It therefore appears that one can consider an aquifer vertically finite, with respect to mixing, when the penetration depth of the diffusive boundary layer is larger than 0.07.

Application of Scaling Analysis to the Geological Storage of CO_2 in Deep Saline Aquifers

Analysis of the conditions that drive convective instability, rate of mixing, and mixing time scales may provide useful input for choosing suitable candidate sites for CO_2 storage. In screening and choosing suitable candidates for large-scale geological CO_2 storage, the onset of convection, rate of mixing of CO_2, and corresponding time scales are quite important. Convective mixing of CO_2 leads to improved dissolution of CO_2 in formation brine, reducing the risk of leakage of CO_2. In the following, the scaling analysis presented in this study is used to conduct a screening assessment of some of the Alberta basin aquifers in Canada.

Acid gases (mixtures of CO_2 and H_2S) are being injected into deep saline aquifers of 24 storage sites in the Alberta Basin, Canada. We have analyzed some of the aquifers of the Alberta Basin as candidates for CO_2 storage by examining the applicability of the presented scaling for the Sherwood number (assuming a homogenous formation; see also Discussion). These saline aquifers are used as an analogue for pure CO_2 storage cases. The Rayleigh numbers for these sites are calculated by Eq. 4 using data provided by Bachu et al.[21] and Bachu and Carroll.[22] The calculated Rayleigh numbers for these aquifers are presented in Table 2. Results show that the calculated Rayleigh numbers are greater than $4\pi^2$ in 14 of the 24 sites investigated. Therefore, >50% of the injection sites would likely undergo convection in the long term, leading to improved dissolution of CO_2. Ten sites indicate pure diffusive mixing, corresponding to cases with low Rayleigh numbers. Finally, in 23 of the 24 cases, the calculated Rayleigh numbers are all well below 600. This suggests that the scaling analysis detailed in this paper can generally be applied to the aquifers studied.

The time to onset of convective mixing, initial wavelength of the convective instabilities, and dissolution of CO_2 at maximum Sherwood number and its corresponding time are calculated for these aquifers and shown in Table 2. Results show that the time for onset of convection varies from 1 to 310 years depending on aquifer properties. The predicted initial wavelengths of the convective instabilities vary from about 2 to about 40 meters. Such small wavelengths pose a numerical challenge in accurately modeling large scale flow simulations in geological formations. Results show that the time for the Sherwood number to reach its maximum varies from a decade to more than 5000 years. Results demonstrate that at the time of maximum Sherwood number, more than 50% of the ultimate dissolution is achieved.

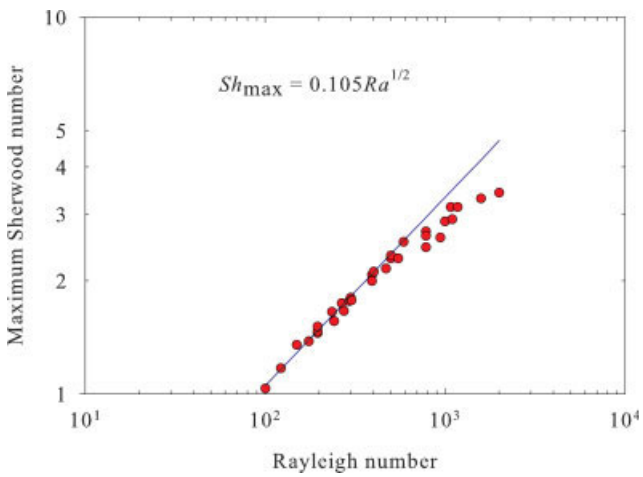

Figure 11. Maximum Sherwood number for different cases studied as a function of Rayleigh number.

[Color figure can be viewed in the online issue, which is available at www.interscience.wiley.com.]

Table 2. Calculated Rayleigh Numbers for 24 Acid Gas Injection Sites in the Alberta Basin

Site	k (mD)	ϕ	μ (mPa s)	$D \times 10^9$ (m^2/s)	$\Delta\rho$* (kg/m^3)	H (m)	Ra	Onset Time (yr)	Wavelength (m)	Time at Sh_{max} (yr)	Mixing at Sh_{max} (%)
1	30	0.06	0.60	4.1	4.7	15	142	44	13	460	0.72
2	186	0.18	0.66	4.0	3.6	10	139	21	9	210	0.72
3	40	0.05	0.78	3.9	1.6	18	74	241	30	1510	0.80
4	100	0.10	0.65	3.7	4.3	8	141	14	7	150	0.72
5	16	0.07	0.64	5.1	1.5	10	11	pd†	–	–	–
6	30	0.12	0.50	5.5	3.2	13	38	pd	–	–	–
7	6	0.13	0.74	3.2	4.4	4	3	pd	–	–	
8	9	0.04	0.67	3.7	4.3	81	318	275	33	5600	0.67
9	6	0.20	0.63	4.2	3.4	29	11	pd	–	–	–
10	9	0.12	0.46	4.5	8.9	9	29	pd	–	–	–
11	137	0.09	0.36	7.6	4.1	60	1359	4	7	–	0.58
12	75	0.06	0.39	7.4	3.4	10	146	10	9	110	0.72
13	115	0.08	0.48	5.0	6.1	10	364	2	4	55	0.66
14	9	0.12	0.44	5.5	6.2	10	19	pd	–	–	–
15	14	0.06	1.32	2.7	0.0	10	0	pd	–	–	–
16	67	0.22	0.82	2.6	6.0	40	351	80	15	1730	0.66
17	346	0.10	0.60	3.7	5.3	4	329	1	1.6	13	0.66
18	10	0.11	0.61	4.5	3.4	24	27	pd	–	–	–
19	13	0.12	0.65	4.3	2.8	13	14	pd	–	–	–
20	32	0.12	0.57	4.3	4.8	13	67	139	25	800	0.83
21	27	0.05	0.63	5.0	1.9	40	127	310	39	3000	0.72
22	109	0.06	0.55	4.6	4.5	5	162	3	4	40	0.71
23	1	0.12	0.48	5.9	3.5	26	3	pd	–	–	–
24	130	0.10	0.52	5.5	2.9	10	133	17	10	170	0.72

*Density difference between CO_2 saturated brine and fresh brine.
†Pure diffusion (no convective mixing).

Discussion

Numerical simulations presented here assume homogenous and isotropic porous media, with no physical perturbations imposed. However, real geological formations are of course not homogenous. Therefore, assuming a single value for the aquifer permeability may well not be representative. It is expected that permeability heterogeneity might have a large effect on the onset time and subsequent growth (or decay) of density-driven instabilities. We speculate that, for real geological formations, where, for example, the permeability variations might trigger perturbations, the onset of convection is different than for homogenous formations. The approximations presented here give insight into understanding the mixing mechanisms for screening appropriate candidates for geological storage of CO_2. More investigation is needed to characterize the effect of permeability field perturbations on the scaling behavior of convective mixing in deep saline aquifers. The scaling presented for the Sherwood number also deviates from the relationship presented at large Rayleigh numbers (Ra > 600), suggesting that the scaling is not applicable for aquifers with large Rayleigh numbers such as Sleipner in the North Sea with Ra $\approx$ 10,000. In addition, we approximated the two-phase flow condition by maintaining a constant boundary condition at the top, which might affect the analysis. Furthermore, three-dimensional effects, geochemical reactions, and aquifer dipping are also neglected, which might alter the evolution of the convective instabilities.

Summary and Conclusions

Prediction of the final fate of the injected CO_2 is necessary for large-scale implementation of CO_2 storage in saline aquifers. Field scale simulations of the convective mixing process are computationally expensive. Therefore, finding simple scaling relationships that characterize the long term behavior of the mixing process are useful for better understanding the final disposition of CO_2 in saline aquifers. In this paper, we have used direct numerical simulations of the convective mixing process to find appropriate scaling relationships for rate of dissolution of CO_2 which can help in the screening of storage sites.

The mixing periods and scaling analysis for the Sherwood number are presented for the first time in this work. The scaling relationships obtained can be used to estimate the onset of natural convection, the approximate size of the convective instabilities, the degree of mixing achieved, and its corresponding time. Such scaling relationships can be used to predict the rate of dissolution of CO_2 and give insight into proper implementation of large-scale geological storage in saline aquifers. The properties of the aquifers in the Alberta Basin studied in this paper are such that most of them fall in the range studied in this work, suggesting that their behavior may be predicted by the sort of analyses performed here. In addition, based on numerical simulation results, a criterion is also presented that give the appropriate numerical grid block size needed for accurate modeling of convective mixing of CO_2 in deep saline aquifers.

Acknowledgments

This work was carried out with financial support from the National Science and Engineering Research Council of Canada (NSERC) and the Alberta Department of Energy. Computer facilities were provided through a CFI grant. The authors acknowledge helpful discussions with Dr. Ali M Saidi, Dr. Tony Settari, Dr. Ayodeji A. Jeje, and Dr. Jalel Azaiez. The authors thank two reviewers for useful comments. The first author also thanks the National Iranian Oil Company (NIOC) for financial support.

Literature Cited

1. Lindeberg EGB, Wessel-Berg D. Vertical convection in an aquifer column under a gas cap of CO_2. *Energy Convers Manage*. 1996;38 (Suppl.):229–234.
2. Neild DA, Bejan A. *Convection in Porous Media*, 2nd ed. New York: Springer-Verlag, 1999.
3. Ennis-King JP, Preston I, Paterson L. Onset of convection in anisotropic porous media subject to a rapid change in boundary conditions. *Phys Fluids*. 2005;17:84107–84115.
4. Ennis-King JP, Paterson L. Role of convective mixing in the long-term storage of carbon dioxide in deep saline formations. *SPE J*. 2005;10:349–356.
5. Riaz A, Hesse M, Tchelepi A, Orr F Jr. Onset of convection in a gravitationally unstable, diffusive boundary layer in porous media. *J Fluid Mech*. 2006;548:87–111.
6. Xu X, Chen S, Zhang Z. Convective stability analysis of the long-term storage of carbon dioxide in deep saline aquifers. *Adv Water Resour*. 2006;29:397–497.
7. Hassanzadeh H, Pooladi-Darvish M, Keith DW. Stability of a fluid in a horizontal saturated porous layer: effect of non-linear concentration profile, initial and initial conditions. *Transp Porous Media*. 2006; 65:193–211.
8. Hassanzadeh H. Mathematical modeling of convective mixing in porous media for geological CO2 storage. Ph.D. Dissertation, University of Calgary, Alberta, Canada, 2006.
9. Aziz K, Settari A. *Petroleum Reservoir Simulation,* 1st ed. London: Elsevier, 1979.
10. Horton CW, Rogers FT Jr. Convection currents in porous media. *J Appl Phys*. 1945;20:367–369.
11. Lapwood ER. Convection of a fluid in a porous medium. *Proc Cambridge Philos Soc*. 1948;44:508–521.
12. Burnett RD, Frind EO. Simulation of contaminant transport in three dimensions 1: the alternate direction Galerkin technique. *Water Resour Res*. 1987;23:689–694.
13. Burnett RD, Frind EO. Simulation of contaminant transport in three dimensions 2 dimensionality effects. *Water Resour Res*. 1987;23: 695–705.
14. Saidi AM. *Reservoir Engineering of Fractured Reservoirs*. Paris: TOTAL Edition Press, 1987.
15. Pooladi-Darvish M. Mathematical modeling of non-isothermal gravity drainage. Ph.D Dissertation, University of Alberta, Canada, 1993.
16. Hassanzadeh H, Pooladi-Darvish M, Keith DW. Modeling of convective mixing in CO_2 storage. *J Can Pet Technol*. 2005;44:43–51.
17. Bird RB, Stewart WE, Lightfoot EN. *Transport Phenomena*. New York: Wiley, 1960.
18. Einstein A. Über die von der molekularkinetischen theorie der wärme geforderte bewegung von in ruhenden flüssigkeiten suspendierten teilchen. *Ann Phys*. 1905;17:549–560.
19. Schlichting H. *Boundary-Layer Theory*. New York: McGraw-Hill, 1955.
20. Carslaw HS, Jaeger JC. *Conduction of Heat in Solids*. Oxford: University Press, 1959.
21. Bachu S, Nordbotten JM, Celia MA. Evaluation of the spread of acid gas plumes injected in deep saline aquifers in western Canada as an analogue to CO_2 injection in continental sedimentary basins. Proceedings of *7th International Conference on Greenhouse Gas Control Technologies*, 5–9 September 2004, Vol. 1, Peer Reviewed Papers and Overviews. In: Rubin ES, Keith DW, Gilboy CF editors. Vancouver, Canada: Elsevier, 2005:479–487.
22. Bachu S, Carroll JJ. In-situ phase and thermodynamic properties of resident brine and acid gases (CO_2 & H_2S) injected in geological formations in western Canada. *Proceedings of 7th International Conference on Greenhouse Gas Control Technologies*, 5–9 September 2004, Vol. 1, Peer Reviewed Papers and Overviews. In: Rubin ES, Keith DW, Gilboy CF editors. Vancouver, Canada: Elsevier, 2005: 449–457.

Manuscript received Oct. 13, 2006, and revision received Feb. 20, 2007.